

Three-dimensional cavity nanoantenna coupled plasmonic nanodots for ultrahigh and uniform surface-enhanced Raman scattering over large area

Wen-Di Li, Fei Ding, Jonathan Hu, and Stephen Y. Chou*

*NanoStructure Laboratory, Department of Electrical Engineering, Princeton University,
Princeton, New Jersey 08544, USA
chou@princeton.edu

Abstract: We propose and demonstrate a new SERS substrate architecture that couples a dense three-dimensional (3-D) cavity nanoantenna array, through nano-gaps, with dense plasmonic nanodots; and a new nanofabrication that combines nanoimprint, guided self-assembly and self-alignment and has fabricated the architecture precisely, simply, inexpensively and over large area (4-inch wafer). We experimentally achieved not only high area-average SERS enhancement (1.2×10^9) but also excellent uniformity (22.4% variation) at the same time over the entire large-area sample by measuring 90 points with a regular mapping distance. The best uniformity achieved is 15% variation over 1.6 mm by 1.6 mm area at slightly lower enhancement factor and is independent of the excitation laser probe size, which had an area varying from ~ 1 to $10,000 \mu\text{m}^2$.

©2011 Optical Society of America

OCIS codes: (240.6695) Surface-enhanced Raman scattering; (250.5403) Plasmonics; (220.4241) Nanostructure fabrication.

References and links

1. M. Fleischmann, P. J. Hendra, and A. J. McQuillan, "Raman-spectra of pyridine adsorbed at a silver electrode," *Chem. Phys. Lett.* **26**(2), 163–166 (1974).
2. D. L. Jeanmaire, and R. P. Van Duyne, "Surface Raman spectroelectrochemistry. 1. heterocyclic, aromatic, and aliphatic-amines adsorbed on anodized silver electrode," *J. Electroanal. Chem.* **84**(1), 1–20 (1977).
3. M. G. Albrecht, and J. A. Creighton, "Anomalously intense Raman-spectra of pyridine at a silver electrode," *J. Am. Chem. Soc.* **99**(15), 5215–5217 (1977).
4. S. M. Nie, and S. R. Emory, "Probing single molecules and single nanoparticles by surface-enhanced Raman scattering," *Science* **275**(5303), 1102–1106 (1997).
5. K. Kneipp, Y. Wang, H. Kneipp, L. T. Perelman, I. Itzkan, R. Dasari, and M. S. Feld, "Single molecule detection using surface-enhanced Raman scattering (SERS)," *Phys. Rev. Lett.* **78**(9), 1667–1670 (1997).
6. N. P. W. Pieczonka, and R. F. Aroca, "Single molecule analysis by surfaced-enhanced Raman scattering," *Chem. Soc. Rev.* **37**(5), 946–954 (2008).
7. D. K. Lim, K. S. Jeon, H. M. Kim, J. M. Nam, and Y. D. Suh, "Nanogap-engineerable Raman-active nanodumbbells for single-molecule detection," *Nat. Mater.* **9**(1), 60–67 (2010).
8. H. Y. H. Chan, C. C. Takoudis, and M. J. Weaver, "High-pressure oxidation of ruthenium as probed by surface-enhanced Raman and X-ray photoelectron spectroscopies," *J. Catal.* **172**(2), 336–345 (1997).
9. S. C. S. Lai, and M. T. M. Koper, "Ethanol electro-oxidation on platinum in alkaline media," *Phys. Chem. Chem. Phys.* **11**(44), 10446–10456 (2009).
10. Z. Q. Tian, and B. Ren, "Adsorption and reaction at electrochemical interfaces as probed by surface-enhanced Raman spectroscopy," *Annu. Rev. Phys. Chem.* **55**(1), 197–229 (2004).
11. X. M. Zhao, B. H. Zhang, K. L. Ai, G. Zhang, L. Y. Cao, X. J. Liu, H. M. Sun, H. S. Wang, and L. H. Lu, "Monitoring catalytic degradation of dye molecules on silver-coated ZnO nanowire arrays by surface-enhanced Raman spectroscopy," *J. Mater. Chem.* **19**(31), 5547–5553 (2009).
12. J. D. Driskell, S. Shanmukh, Y. J. Liu, S. Hennigan, L. Jones, Y. P. Zhao, R. A. Dluhy, D. C. Krause, and R. A. Tripp, "Infectious agent detection with SERS-active silver nanorod arrays prepared by oblique angle deposition," *IEEE Sens. J.* **8**(6), 863–870 (2008).
13. I. S. Patel, W. R. Premasiri, D. T. Moir, and L. D. Ziegler, "Barcoding bacterial cells: A SERS based methodology for pathogen identification," *J Raman Spectrosc* **39**(11), 1660–1672 (2008).

14. R. A. Tripp, R. A. Dluhy, and Y. P. Zhao, "Novel nanostructures for SERS biosensing," *Nano Today* **3**(3-4), 31–37 (2008).
15. K. A. Willets, and R. P. Van Duyne, "Localized surface plasmon resonance spectroscopy and sensing," *Annu. Rev. Phys. Chem.* **58**(1), 267–297 (2007).
16. M. J. Natan, "Surface enhanced Raman scattering," *Faraday Discuss.* **132**, 321–328 (2006).
17. T. Xiao, Q. Ye, and L. Sun, "Hunting for the active sites of surface-enhanced Raman scattering: A new strategy based on single silver particles," *J. Phys. Chem. B* **101**(4), 632–638 (1997).
18. Y. Fang, N. H. Seong, and D. D. Dlott, "Measurement of the distribution of site enhancements in surface-enhanced Raman scattering," *Science* **321**(5887), 388–392 (2008).
19. M. Kerker, D. S. Wang, and H. Chew, "Surface enhanced Raman scattering (SERS) by molecules adsorbed at spherical particles: errata," *Appl. Opt.* **19**(24), 4159–4174 (1980).
20. S. Panigrahi, S. Prahara, S. Basu, S. K. Ghosh, S. Jana, S. Pande, T. Vo-Dinh, H. Jiang, and T. Pal, "Self-assembly of silver nanoparticles: synthesis, stabilization, optical properties, and application in surface-enhanced Raman scattering," *J. Phys. Chem. B* **110**(27), 13436–13444 (2006).
21. G. Braun, S. J. Lee, M. Dante, T. Q. Nguyen, M. Moskovits, and N. Reich, "Surface-enhanced Raman spectroscopy for DNA detection by nanoparticle assembly onto smooth metal films," *J. Am. Chem. Soc.* **129**(20), 6378–6379 (2007).
22. A. Tao, F. Kim, C. Hess, J. Goldberger, R. He, Y. Sun, Y. Xia, and P. Yang, "Langmuir-Blodgett silver nanowire monolayers for molecular sensing using surface-enhanced Raman spectroscopy," *Nano Lett.* **3**(9), 1229–1233 (2003).
23. A. Gopinath, S. V. Boriskina, B. M. Reinhard, and L. Dal Negro, "Deterministic aperiodic arrays of metal nanoparticles for surface-enhanced Raman scattering (SERS)," *Opt. Express* **17**(5), 3741–3753 (2009).
24. J. Li, H. Lu, W. C. Luk, J. T. K. Wan, and H. C. Ong, "Studies of the plasmonic properties of two-dimensional metallic nanobottle arrays," *Appl. Phys. Lett.* **92**(21), 213106 (2008).
25. X. Y. Zhang, C. R. Yonzon, and R. P. Van Duyne, "Nanosphere lithography fabricated plasmonic materials and their applications," *J. Mater. Res.* **21**(5), 1083–1092 (2006).
26. P. J. Schuck, D. P. Fromm, A. Sundaramurthy, G. S. Kino, and W. E. Moerner, "Improving the mismatch between light and nanoscale objects with gold bowtie nanoantennas," *Phys. Rev. Lett.* **94**(1), 017402 (2005).
27. S. Wang, D. F. P. Pile, C. Sun, and X. Zhang, "Nanopin plasmonic resonator array and its optical properties," *Nano Lett.* **7**(4), 1076–1080 (2007).
28. N. Perney, F. García de Abajo, J. Baumberg, A. Tang, M. Netti, M. Charlton, and M. Zoorob, "Tuning localized plasmon cavities for optimized surface-enhanced Raman scattering," *Phys. Rev. B* **76**(3), 035426 (2007).
29. W. D. Li, and S. Y. Chou, unpublished, 2008.
30. S. Y. Chou, P. R. Krauss, and P. J. Renstrom, "Imprint of sub-25 nm vias and trenches in polymers," *Appl. Phys. Lett.* **67**(21), 3114–3116 (1995).
31. W. Wu, B. Cui, X. Y. Sun, W. Zhang, L. Zhuang, L. S. Kong, and S. Y. Chou, "Large area high density quantized magnetic disks fabricated using nanoimprint lithography," *J. Vac. Sci. Technol. B* **16**(6), 3825–3829 (1998).
32. M. D. Austin, H. X. Ge, W. Wu, M. T. Li, Z. N. Yu, D. Wasserman, S. A. Lyon, and S. Y. Chou, "Fabrication of 5 nm linewidth and 14 nm pitch features by nanoimprint lithography," *Appl. Phys. Lett.* **84**(26), 5299–5301 (2004).
33. K. L. Kelly, E. Coronado, L. L. Zhao, and G. C. Schatz, "The optical properties of metal nanoparticles: The influence of size, shape, and dielectric environment," *J. Phys. Chem. B* **107**(3), 668–677 (2003).
34. A. Christ, G. Lévêque, O. J. F. Martin, T. Zentgraf, J. Kuhl, C. Bauer, H. Giessen, and S. G. Tikhodeev, "Near-field-induced tunability of surface plasmon polaritons in composite metallic nanostructures," *J. Microsc.* **229**(2), 344–353 (2008).

1. Introduction

Surface-enhanced Raman scattering (SERS) [1–3] potentially have enormous applications in many areas of chemical and biological sensing, including single molecule detection [4–7], non-intrusive study of reaction dynamics [8–11], and identification of trace amounts of biological pathogens and dangerous chemical species [12–14], to name a few. The fundamental physics of SERS (dominantly by a local electromagnetic (EM) enhancement and weakly by chemical enhancement) [2,15,16] has been extensively studied and generally understood, and high SERS enhancements have been observed at certain spots of a substrate [4–6,17]. However, despite enormous efforts over many years, two central challenges, which hamper SERS applications, remain unsolved: how to significantly increase the area-average SERS enhancement, and how to overcome the "sparse hot-spots" problem (the SERS enhancement is high only at a few random spots) [18].

The failure to solve the above challenges comes from three aspects. First, the area-average SERS enhancement and large-area uniformity involve multiple physical processes/parameters, how to optimize them and what should be the SERS substrate architectures for such

optimization are still open questions. Second, the SERS dependence on the fourth power of the local electric field enhancement makes it extremely sensitive to the nanofabrication accuracy and hence hard to control when structures are extremely small. Therefore it is an open question that what should be the high-precision nanofabrication technology and which SERS substrate architecture can lessen the sensitivity of the area-average SERS enhancement and uniformity to the nanofabrication errors. And third, since electron beam lithography (EBL) has limited area and throughput, it is also unclear what should be the technology for fabricating SERS substrates over large area.

For examples, most of the traditional and commonly-used SERS substrate architectures are solely based on the local electric field enhancement from the sharp edges or the small gaps (between two metallic nanostructures) of either roughened metallic surfaces [1–3] or metallic nanoparticles randomly deposited on a surface [19–22]. The highest SERS enhancement has been found to be in the smallest gap between two metallic nanostructures, rather than near a sharp edge of an isolated nanostructure [17]. However in these substrates, the high SERS enhancement occurs only at sparse hot-spots while the area-average is extremely low [17] due to the broad and random distribution in nanoparticle/edge's size, gap, and location which makes it difficult to meet the stringent requirements for high SERS enhancement. To overcome the randomness, lithography methods (e.g. nanosphere lithography, interference lithography, EBL, etc) have been used to pattern nanostructures [23–25], yet achieved limited success due to the insufficient resolution of these lithography methods in controlling the geometry.

Another important factor to SERS enhancement, which has been ignored for two decades, is the efficiency in collecting the excitation light and radiating Raman signal. The nanoparticles are intrinsically poor light absorbers and radiators, because their sizes are much smaller than the excitation and radiation light wavelength [26]. Thus, for the incoming excitation light and outgoing Raman signal, only a tiny portion of them was absorbed and radiated respectively, greatly reducing the SERS enhancement. To solve this issue, a planar (i.e. two-dimensional (2-D)) bowtie antenna array, each with a single small gap, was proposed and fabricated by EBL [26]. However, the SERS enhancement is not very high and the “sparse hot-spots” problem still exists, because (a) EBL does not have a sufficient resolution to make the a few nanometer gaps and make them accurately, and (b) even if every gap is “hot,” the planar 2-D antenna architecture intrinsically has a very low density of the SERS active region (gaps).

More recently, a third approach to SERS substrate is that it does not use any gaps at all but a 3D metallic resonant cavity (antenna) for improving SERS signal uniformity. When designed properly, such cavity antennas solely depend on the cavity to effectively absorb and trap the incoming light to increase SERS enhancement. The examples of such cavities include the inverted pyramids and the nanopin [27,28]. Because these cavity antennas do not have any small gaps for enhancing local E-field, their SERS enhancement is limited. Furthermore, currently these antenna have a unit cell of 1-2 μm pitch, which is comparable to a diffraction-limited excitation laser probe spot size, leading to a large signal variation unless the laser probe area is expanded to tens of microns diameter, which could significantly slows down the measurement speed [28].

2. New SERS substrate architecture: 3-D cavity nanoantenna coupled with plasmonic nanodots through nanogaps

Our SERS architecture puts dense plasmonic nanodots inside dense a 3-D cavity nanoantenna array and couples the nanoantennas with the nanodots as well as the nanodots themselves through nanogaps. One implementation of such architecture is the structure, termed “disk-coupled dots-on-pillar antenna-array” (D2PA), that has a high-density and high-efficiency 3-D cavity nanoantenna array coupled with, through nanometer gaps, high-density plasmonic nanodots (Fig. 1) [29]. The 3-D cavity antenna array consists of a periodic dielectric pillar array on a substrate with a metal disk on top of each pillar and a metal back-plane on the bottom side of the pillars (each disk is exactly aligned with a hole in the backplane, as

discussed in fabrication). The disks and the backplane provide a vertical cavity for the light, while the periodic structure forms a lateral cavity. The dense metal nanodots are on the sidewall of each pillar with a small gap between the edge of the disk and the nanodots as well as between the neighboring nanodots.

The 3-D nanoantenna array plays the role of (a) collecting the incident light and focusing it into the nanogaps, (b) increasing the total absorption of excitation light through the cavities, and (c) increasing the efficiency of the Raman signal radiation. The plasmonic nanodots are for creating high local fields using their small gaps with the antenna's (disk) edge and

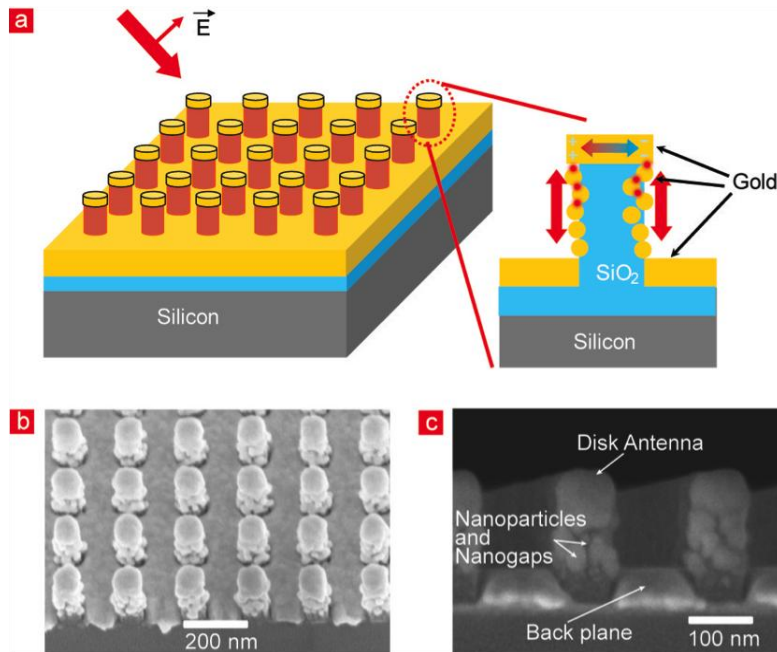


Fig. 1. Disk-coupled dots-on-pillar antenna (D2PA) structure for surface enhanced Raman scattering. (a) Schematic; (b) top-view scanning electron micrograph (SEM); and (c) cross-sectional SEM of a D2PA structure, which consists of dense 3-D cavity nanoantennas (a metal disk array and a metal backplane on the top and the foot of the SiO_2 pillars respectively) coupled to, through nanogaps, dense plasmonic nanodots on the SiO_2 pillars' sidewall inside the cavity.

themselves and using the nanodots' sharp edges. The high density of the nanodots on each pillar increases the total number of SERS active spots and also reduces SERS signal's statistic variation. The 3-D arrangement allows both nanodots and nanoantenna having a high density than a 2-D structure, hence further increasing the SERS enhancements. Moreover, as discussed later, the D2PA architecture has its SERS enhancement relatively insensitive to certain fabrication variations, and can be fabricated precisely and simply by a new fabrication method.

An example of the D2PAs we fabricated consists of a round SiO_2 pillar of 70 nm diameter and 130 nm height on a silicon substrate (Fig. 1b and 1c). The metallic disks, back-plane, and nanodots are all made of Au with a disk diameter of ~ 100 nm, a disk and back-plane thickness of 50 nm, and an average nanodot diameter of ~ 30 nm. Clearly shown in the scanning electron microscope (SEM) image (Fig. 1c), the gap between the disk and dots as well as between the dots varies from ~ 1 to 10 nm. For this particular structure, the average number of gold nanodots next to each disk antenna and on the entire pillar is estimated to be approximately 7 and 20 respectively.

To get large SERS enhancements, we need to optimize the small gaps, the sharp edges, the matching of the substrate surface plasmon frequency with the excitation light wavelength, the efficiency for each nano-antennas, the effective coupling between the nano-antenna and the gaps, the vertical and lateral resonant cavity to improve the light absorption and radiation, the number of nano-antennas per unit area, and the number of SERS effective nanogaps per unit area.

Clearly, the D2PA architecture not only has combined the advantages of sharp edges, small gaps, antenna, and cavity (which used to be used separately) in one SERS structure, but also allow high antenna density, high hot spot density, less sensitivity to fabrication errors and easy fabrication (see below for the last two).

3. Nanofabrication combining nanoimprint with guided self-assembly

The D2PA was fabricated on 4" wafers by a new nanofabrication approach that combines nanoimprint (top-down) [30] with guided self-assembly (bottom-up). The nanoimprint was used to fabricate the 3-D cavity antenna and the pillar template that was later used to guide the self-assembly of the metal dots and the small gaps. The nanoimprint molds were fabricated without using EBL and have a size of 4 inch [31]. Such fabrication approach can be extended to substrates much larger than 4 inch.

In one of our fabrications, the pillars were patterned first in a SiO₂ layer grown on Si by nanoimprint and reactive ion etching [31]. Then a thin gold layer was evaporated onto the wafer in a direction normal to the wafer surface, which simultaneously deposited the gold on the pillar top, the backplane, and the pillar sidewall. Guided by the SiO₂ pillars, the gold deposited on the pillar top and the pillar foot formed the disks and the backplane respectively, but on the pillar sidewall the gold self-assembled into nanodots with a small gap in between and self-aligned precisely next to the metal disk (antenna). The gold self-assembly on the sidewall is a result of the non-wetting property of gold on SiO₂ surface, the gold diffusion at the elevated evaporation temperature, and the thin gold layer thickness.

The new fabrication approach is much simpler yet more precise than other fabrication approaches. Not only it involves just a few steps, but also nanoimprint offers sub-2 nm duplication accuracy [30,32], self-assembly offers a few nm gap and dense nanodot (which are unachievable with current EBL or other writing based lithography.) The guiding in the self-assembly "self-aligned" the nanodots at the "exact" desired locations without having any additional precision alignment in lithographies (one of the biggest challenges in nanofabrication.)

4. Characterization of SERS enhancement factors

We have extensively studied the effects of various parameters of the D2PA on SERS by fabricating the D2PA with different geometries and materials, measuring SERS enhancements in the Raman spectrum of trans-1,2-bis(4-pyridyl)ethylene (BPE) molecules adsorbed on the D2PA surface (mainly by comparing the intensities of the BPE's 1200 cm⁻¹ peaks), and modeling with finite-difference time-domain (FDTD) methods. All D2PAs studied in this paper have used the nanoantenna array of a 200 nm period.

We diced the large-area SERS substrate into small pieces of approximately 3 mm by 3 mm, and each piece was chemically pre-treated before analyte molecules were deposited and measured. 0.182 g purified BPE was dissolved in 10 mL ethanol to form 100 mM solution, which was then stepwise diluted to lower concentrations for SERS measurement. 2 μL BPE solution was dropped on SERS samples using an accurate pipette, and then dried in air with gentle nitrogen blow to obtain a uniform molecule deposition. This treatment enables us to accurately control the total molecule numbers deposited on the SERS substrate surface with known concentration, volume, and sample area. To calculate the enhancement on our SERS samples, a piece of control sample without Raman enhancement, which has 50 nm aluminum deposited on a flat glass slide by e-beam evaporation at 0.6 Å/s, was also processed in the same way described above as the SERS samples as a reference.

The SERS enhancements of the BPE absorbed on our samples were measured using a commercial confocal Raman microscope equipped with a 785 nm laser (ARAMIS by Horiba) and was compared with the aluminum reference substrate which is assumed no enhancement to Raman signal. In our work, the analytical enhancement factor is defined as $EF = \frac{I_{SERS}}{I_{REF}} \cdot \frac{C_{REF} \cdot P_{REF} \cdot T_{REF}}{C_{SERS} \cdot P_{SERS} \cdot T_{SERS}}$, where I_{SERS} and I_{REF} is the measured Raman intensity, C_{SERS} and C_{REF} is the concentration of BPE solutions dropped, P_{SERS} , P_{REF} , T_{SERS} and T_{REF} is the excitation power and exposure time, respectively on the D2PA SERS substrate and the reference substrate.

In the calculation of enhancement factors, I_{SERS} and I_{REF} are measured as the area under BPE's 1200 cm^{-1} Raman peak fitted from the baseline-removed Raman spectra using a Gaussian-Lorentzian lineshape. In order to achieve comparable Raman signal intensities on various samples with significantly different Raman signal enhancements, we used different excitation powers and exposure times on different D2PA and the reference measurements. Moreover, BPE solutions applied onto the D2PA and the reference substrates have different concentrations, i.e., 1 μM on all D2PA substrates comparing with 100 mM on reference substrates. The measured Raman intensities were normalized with specific experimental parameters used in each measurement. To avoid introducing measurement errors, the microscope lens and other experimental setups are all fixed.

To handle the potential non-uniformity in the BPE molecules deposited on the reference sample due to a possible recrystallization caused by a high concentration BPE solution, we measured 400 points uniformly covering the whole reference sample area to obtain an average Raman intensity as the reference used in the enhancement factor calculation.

Our Horiba Raman microscope has both (a) laser beam raster-scanning over a sampling area and (b) stage scanning over an entire sample, together (controlled by software) providing a powerful tool to examine the SERS enhancement uniformity of the entire sample. The laser beam scanning area covers from the laser spot size of $\sim 1 \mu\text{m}^2$ (stationary) to a square area up to 100 μm by 100 μm (raster-scan). The stage scan covers an area of up to 20 mm by 20 mm using x and y axis stepping.

Some of our major findings are given below.

5. Results and discussion

5.1 High and uniform SERS enhancement factors over large area on D2PAs

Through systematically experimental study and optimization of D2PA's different parameters (see section 5.2-5.6), we have achieved an *area-average* SERS enhancement of (i) 1.2×10^9 over the entire pattern area (total 90 measurement points) with a variation of 22.4% (defined as the ratio between the standard deviation and the mean value of the measured Raman signal intensities) for the D2PA with elliptical shape pillars (120 nm long, 65 nm wide, 55 nm pillar height, and 50 nm thick Au, Fig. 2a and 2c); and (ii) 3.1×10^8 over the entire sample (1.6 mm by 1.0 mm and total 160 measurement points) with uniformity of 25% variation on the D2PA with round shape pillars (130 nm disk diameter, 55 nm pillar height, and 50 nm thick Au, Fig. 2a and 2b). We attribute a higher SERS enhancement in the D2PA of elliptical pillars to a better match between the plasmon resonant wavelength and the excitation laser [33] and to a sharper structure edge.

It is important to note the achieved excellent uniformity of high SERS enhancement over large area. Lacking such uniformity has hampered many SERS applications previously. For

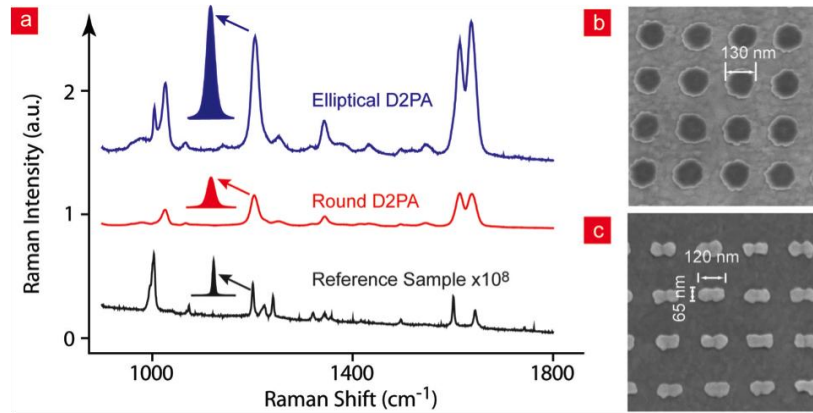


Fig. 2. Experimental high area-average SERS enhancement factor for BPE. (a) Typical experimental Raman spectra on a D2PA substrate with round pillars (red) and with elliptical pillars (blue), and on a reference flat substrate (black and its signal scaled up by 10^8). Comparison of the areas under the BPE's 1200 cm^{-1} peaks gives an enhancement factors of 3.1×10^8 and 1.2×10^9 for D2PA substrates with the round and elliptical pillars respectively; (b) and (c), top-view SEMs of the two different D2PA substrates.

the D2PA with elliptical shape pillars, the pillars with optimized elliptical long and short axis are in $4.5\text{ }\mu\text{m}$ by $4.5\text{ }\mu\text{m}$ patches repeating every $45\text{ }\mu\text{m}$ over $4''$ wafer area which was fabricated by a special EBL-free lithography method (to be reported elsewhere). For each pattern area ($4.5\text{ }\mu\text{m}$ by $4.5\text{ }\mu\text{m}$), we measured 9 data points using a $1.5\text{ }\mu\text{m}$ by $1.5\text{ }\mu\text{m}$ beam size at a step distance of $1.5\text{ }\mu\text{m}$. A typical SERS enhancement variation in a patch is shown in Fig. 3c. We measured total 10 pattern areas, hence a total of 90 data points, and have their

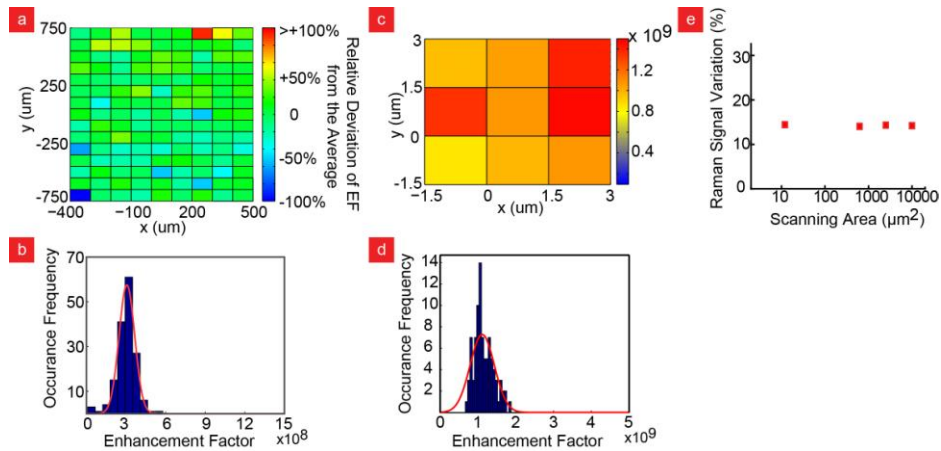


Fig. 3. Experimental uniformity of high SERS enhancement over large area. The mapping (a) and the histogram (plus the Gaussian fitting) (b) of the SERS enhancements of an optimized D2PA substrate (130 nm diameter round pillars) of 1.6 mm by 1.0 mm area using a laser spot size of $20\text{ }\mu\text{m}$ by $20\text{ }\mu\text{m}$ and a step of $100\text{ }\mu\text{m}$ (hence 160 sampling points), showing an average SERS enhancement of 3.1×10^8 and a variation of 25%; (c) and (d), the mapping and histogram of SERS enhancements on a special D2PA substrate (elliptical pillars) of multiple $4.5\text{ }\mu\text{m}$ by $4.5\text{ }\mu\text{m}$ pattern areas using a laser spot size of $1.5\text{ }\mu\text{m}$ diameter and a step size of $1.5\text{ }\mu\text{m}$ (hence 9 sampling points for a given area in (c)), but the histogram and enhancement variation calculation are based on the measurements of the 10 identical pattern areas (total 90 points) on the same sample (d.), showing an average SERS enhancement of 1.2×10^9 and a variation of 22.4%; (e) the variation of SERS enhancement versus excitation laser spot size on a D2PA substrate with the round pillars and an area-average of SERS of 1.6×10^7 over an area of 1.6 mm by 1.6 mm .

distribution in Fig. 3d, which gives area-average SERS enhancement of 1.2×10^9 with the variation is 22.4%.

For the round shape D2PA structure, they are uniform over whole 4" wafer area. We measured the uniformity by scanning point-to-point over the entire area of 1.6 mm by 1.0 mm using 20 μm by 20 μm probe area size and at a step distance of 100 μm (hence total 160 measurement points over the entire sample were used in calculation), giving an area-average SERS enhancement of 3.1×10^8 with the variation of 25% (Fig. 3a and 3b). The scanned area is slightly smaller than the total sample area to exclude the areas damaged by the sample handling with tweezers.

Furthermore, we varied the equivalent laser probe spot size by raster-scanning the laser beam within a predefined probe area and found that the variation of the area-average SERS enhancement in our D2PA samples is independent of the equivalent excitation laser beam spot sizes we used. For example, for a D2PA with round pillars and an average of SERS enhancement factor of 1.6×10^7 , when the probe area is changed from ~ 1 to 10,1000 μm^2 and the stage scan is 1.6 mm by 1.6 mm at the center of a 3 mm by 3mm sample (measured 64 points at a 200 μm step), the SERS enhancement variation stays at a constant 15% (Fig. 3e).

5.2 Effects of nanodots

We studied the effect of the nanodots on SERS enhancement by making the D2PA samples with and nearly without nanodots in the same fabrication except one step. The SERS measurements show that the D2PA with nanodots has a SERS enhancement ~ 7 times higher than that nearly without nanodots (Fig. 4a). We attribute the higher SERS enhancement to a significantly higher local electrical field generated between the disk rim and a nanodot and between nanodots.

To further investigate the effects of the nanodots, we used numerical simulation with a commercial 3-D finite-difference time-domain (FDTD) solver from Lumerical Solutions. In the simulation, the incident plane wave propagates from the top of the D2PA normal to the nanodisks and the polarization aligns with the nanodots on the pillar sidewall (Fig. 4b), and the refractive indices of gold was the experimentally measured values. The thickness of the gold nanodisk and gold back plane is 50 nm. The diameters of the pillar and the nanodisk are 70 nm and 100 nm, respectively. The ellipsoidal nanodot on the side wall of the pillar has diameters of 15 nm, 30 nm, and 30 nm in x, y, and z directions, respectively (x direction is normal to pillar sidewall and z direction is the normal of the sample surface). The gap between the nanodot and nanodisk is 3 nm. Two nanodots are placed symmetrically on each

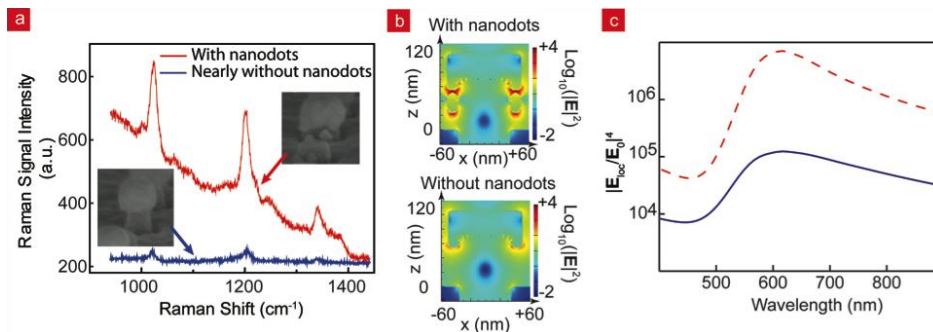


Fig. 4. Comparison of Raman signals from D2PA samples with dots and nearly no dots. (a) Experimental Raman spectrum of BPE molecules adsorbed on the D2PA samples with nanodots shows approximately 7 times stronger signal than that from the D2PA samples with nearly no dots. (b) FDTD simulation shows that the electrical field around the disk is significantly stronger in the D2PA with nanodot than that without nanodots. (c) The 4th power of the ratio of local electrical field (midway between the disk and the nanodot) to the incident field as a function of incident light wavelength. The simulation also shows the resonant wavelength of the D2PA does not change much with the existence of nanodots.

pillar sidewall in the x direction, which is the same as the incident polarization direction. The simulation of the fourth order of the local field enhancement versus incident wavelength (Fig. 4c) shows that the simulated local enhancement at the midpoint of the gap is two orders of magnitude higher in the structure with the nanodots than without the nanodots. Note that the enhancement at the midpoint is the highest in a SERS structure, and the experiment measures the average local field enhancements over the entire probe area rather than a point, hence the measured average enhancement (which is 7 in our case) is much less than the simulated enhancement at the middle of the gap.

Another important finding in our simulation is that the resonant frequency of a D2PA for the EM enhancement, which is defined as the frequency/wavelength that gives the highest electrical field at the midpoint between the disk rim and the neighboring nanodot, is nearly independent of the size and the number of nanodots or the size of nanogaps, but the disk diameter (Fig. 4c). We attribute this mainly to the 3-D arrangement of the nanodisks and the nanodots. Since the nanodots are underneath and blocked by the nanodisk antenna, the interaction between the incident light and the nanodisk antenna is dominant and the size of the nanodisk is the key factor to determine the resonance frequency of the D2PA structure. This finding is significant for achieving a high SERS enhancement, lessening the SERS enhancement sensitivity to the structure variation, and minimizing the “sparse hot-spots” problem, as discussed later.

5.3 Effects of disk diameter

The disk diameter effects on SERS enhancement were studied by fabricating D2PA samples with disk diameters ranging from 50 nm to 190 nm while fixing the pitch at 200 nm and the pillar height at 130 nm. Raman measurements were conducted at both 632 nm and 785 nm excitation wavelengths respectively (Fig. 5). At 632nm excitation, the strongest enhancement was observed on 110 nm diameter D2PA structures while this optimal diameter shifted to 130 nm for a 785 nm excitation. A similar trend was also seen in our simulation of the electric field at the midpoint between the disk and a nanodot. We attribute the strongest SERS enhancement to the matching between the plasmon resonant wavelength and the excitation laser wavelength. It makes sense that for a fixed disk thickness, a larger disk diameter has a

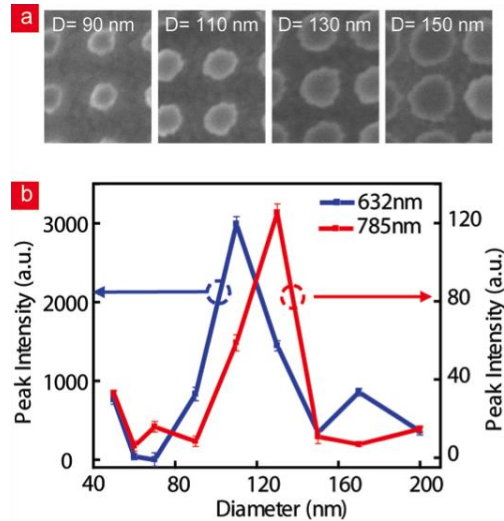


Fig. 5. Experimental Raman signal intensity of BPE's 1200 cm^{-1} peak versus the nanodisk diameter on D2PA substrates. (a) Top-view SEMs of D2PA structures with different disk diameters. (b) The BPE's 1200 cm^{-1} peak intensity versus the nanodisk diameter at 632 nm and 785 nm laser excitation wavelengths respectively.

larger aspect ratio and hence a longer plasmon resonant wavelength.

The experiments further show that a change of the disk average diameter by ± 20 nm (without changing other parameters) causes a change in SERS enhancement of $10 \times (1,000\%)$, giving an average $\sim 50\%$ change per 1 nm error (i.e. $\sim 1\%$ relative error) in the disk diameter. For a disk diameter of ~ 100 nm, nanoimprint offers 1-2 nm duplication accuracy. This means D2PA architecture is far less sensitive to the fabrication error and intrinsically favor deterministic SERS enhancement and large-area uniformity.

5.4 Effects of pillar height

We investigated the effect of the pillar height on SERS enhancement by fabricating D2PA structures with different SiO_2 pillar heights while fixing the disk diameter at 100 nm and the gold thicknesses at 50 nm (Fig. 6). As the pillar height is reduced from 86 nm, the Raman signal (hence the enhancement factor) increases gradually, and reaches the highest intensity (increased more than 100%) at the pillar height of ~ 55 nm, giving an average 6% change in the SERS enhancement per 1 nm change in pillar height.

We attribute the pillar height effect to a dominant coupling between the disk and the backplane. We noticed that at the pillar height that gives the highest enhancement, the gap between the top disk and backplane becomes very small and comparable to the gap between nanodots on the sidewall, therefore significantly increase the backplane's contributions to the SERS enhancement. Further lowering pillar height below 55 nm will likely induce electrical shorting between the top nanodisk antenna and the backplane, therefore causing the Raman signal to drop significantly, as we have observed experimentally.

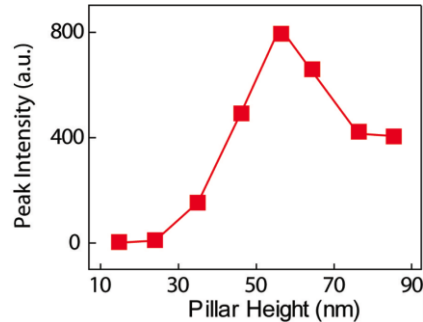


Fig. 6. Experimental Raman signal intensity of BPE's 1200 cm^{-1} peak versus the pillar height of D2PA substrate. The max intensity is observed at 55 nm pillar height and is approximately two times stronger than at 85 nm pillar height.

5.5 Effects of backplane

The backplane plays an important role in the SERS enhancement observed in the D2PA. First, the metal backplane and the metal disks form a vertical plasmonic cavity, which helps collecting the incident excitation light and radiating Raman signal. Second, the metal backplane can enhance the electrical field near the disk. And third, the backplane also can help lateral coupling between the pillars. All factors can contribute to enhance SERS signal. Our FDTD simulation shows that for the pillar with a single dot and 3 nm gap and the gap between gold disk and gold back plane of 70 nm., the $|\mathbf{E}_{\text{loc}}/\mathbf{E}_0|^4$ (where \mathbf{E}_{loc} and \mathbf{E}_0 are the local electric field at the middle of the gap and the incident light respectively) is six times higher with the metal backplane than without (Fig. 7). The simulation also shows that the resonant peak has a slight red shift when the metal back plane is used. The simulated red shift is less prominent than that in case of metal nanowire array with a metal back plane [34], because of less coupling (i.e. larger spacing between the front plane and the back plane).

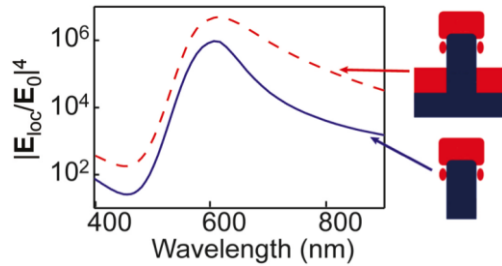


Fig. 7. FDTD simulation of backplane effect. The 4th power of the ratio of local electrical field (midway between the disk and the nanodot) to the incident field as a function of incident light wavelength, showing the D2PA substrates with the gold backplane can be over an order of magnitude higher for that without the backplane.

5.6 Surface plasmon resonant frequency and fabrication requirements

To achieve a high and uniform SERS enhancement, it is essential to have a new SERS substrate architecture that is far less sensitive to fabrication errors than the current architectures. For examples, in nanoparticle-based SERS substrates, it is well known that the plasmon resonant frequency is very sensitive to the dot size, the nanogap size, and the number of nanodots, and hence is very difficult to control, because 1 nm fabrication variation, which is hard to achieve [16], already presents tens percent variation in size for a 10 nm nanodot size and sub-5 nm gap size.

On the other hand, the resonant frequency of in the D2PA, which is primarily determined by the disk diameter but not the dot size, dot number, and gap size, is much easier to control by fabrication. A few nanometer fabrication variation for a disk size of ~100 nm (about one order of magnitude or more larger than the nanoparticles) means only a few percent in relative disk size changes and can be satisfied in the fabrication such as nanoimprint.

6. Conclusion

In summary, we have proposed and demonstrated a new SERS substrate architecture and a new nanofabrication for the architecture, which have led to the achievement of an area-average SERS enhancement of 1.2×10^9 and large-area uniformity with the variation of less than 25%. The new SERS substrate architecture considers the factors of high antenna efficiency, high antenna density, high nanodot density (for both high SERS signal and less statistical variations), better antenna-nanodot coupling, and less sensitivity to fabrication variation into consideration, in additional to the traditional consideration of small gaps and sharp edges. The SERS substrate architecture has been implemented into a structure, D2PA, which has a 3-D resonant cavity antenna (disk-backplane for vertical cavity and periodic structure for lateral cavity) of high density (due to 3-D structure and small foot-print) coupled to dense nanodots effectively (through small nanogaps). The plasmon resonant frequency of the D2PA was found to be primarily dependent on the disk diameter, nearly independent on the size and number of the nanodots and the nanogap, and weakly dependent on the pillar height (for taller pillar). Since the disk diameter is an order of magnitude larger than the nanodots, the SERS enhancement in the D2PA architecture is less sensitive to the fabrication error than conventional nanoparticle based SERS substrates. The new nanofabrication approach, which is simple, no alignment, no EBL, yet precise and suited for large area, uses nanoimprint to fabricate the 3-D cavity antenna and the templates (pillar) for guiding self-assembly of nanodots and the guided self-assembly to create the metal dots and the small gaps and self-align them with the antennas. We believe the results presented here can be further improved. And both new SERS architecture and new fabrication method can be generalized to future design and fabrication of other high and uniform SERS substrates and new plasmonic systems, and significantly advance the application of SERS and other plasmonic effects.

Acknowledgement

W.D.L designed and made the first D2PA sample. W.D.L and F.D contributed to D2PA substrates fabrication and SERS measurements. S.Y.C and W.D.L contributed to the SERS design strategy. J.H contributed to simulation. W.D.L, F.D. J.H. and S.Y.C. contributed to data analysis and manuscript preparation. S.Y.C. designed and directed the research, led the formation and development of the new SERS design strategy, and performed majority writing in the manuscript. The authors thank Dr. Xing Wang for helping on preparation of BPE solutions and other useful discussion, Dr. Zengli Fu for discussion on molecule adsorption, Professor Stephen Lyon for discussing the naming of the D2PA, Dr. Orest J. Glembocki and Dr. Joshua Caldwell of Naval Research Laboratory and Prof. Szymon Suckewer, Dr. Hui Xia and Mr. Chao Lu of Princeton University for Raman measurements of preliminary tests of our early D2PA samples (Note all the data presents here are measured in our group), and Dr. Weihua Zhang for discussion and comments on the manuscript. We thank the Defense Advanced Research Projects Agency (DARPA) (Managed by Dr. Dennis Polla) for its partial support.